biomedicines

MDPI

Article

Cannabidiol Selectively Binds to the Voltage-Gated Sodium Channel $Na_v1.4$ in Its Slow-Inactivated State and Inhibits Sodium Current

Chiung-Wei Huang [1,2], Pi-Chen Lin [3], Jian-Lin Chen [4] and Ming-Jen Lee [5,*]

1 Department of Post Baccalaureate Medicine, Kaohsiung Medical University, Kaohsiung 80708, Taiwan; g10054b@kimo.com
2 Department of Physiology, Kaohsiung Medical University, Kaohsiung 80708, Taiwan
3 Department of Internal Medicine, Division of Endocrinology and Metabolism, Kaohsiung Medical University Hospital, Kaohsiung 80708, Taiwan; pichli@kmu.edu.tw
4 Department of Physiology, National Taiwan University College of Medicine, Taipei 100233, Taiwan; r07441009@g.ntu.edu.tw
5 Department of Neurology, National Taiwan University Hospital, Taipei 100233, Taiwan
* Correspondence: mjlee@ntu.edu.tw; Tel.: +886-2-2312-3456 (ext. 65336)

Abstract: Cannabidiol (CBD), one of the cannabinoids from the cannabis plant, can relieve the myotonia resulting from sodium channelopathy, which manifests as repetitive discharges of muscle membrane. We investigated the binding kinetics of CBD to $Na_v1.4$ channels on the muscle membrane. The binding affinity of CBD to the channel was evaluated using whole-cell recording. The CDOCKER program was employed to model CBD docking onto the $Na_v1.4$ channel to determine its binding sites. Our results revealed no differential inhibition of sodium current by CBD when the channels were in activation or fast inactivation status. However, differential inhibition was observed with a dose-dependent manner after a prolonged period of depolarization, leaving the channel in a slow-inactivated state. Moreover, CBD binds selectively to the slow-inactivated state with a significantly faster binding kinetics (>64,000 M^{-1} s^{-1}) and a higher affinity (K_d of fast inactivation vs. slow-inactivation: >117.42 μM vs. 51.48 μM), compared to the fast inactivation state. Five proposed CBD binding sites in a bundle crossing region of the $Na_v1.4$ channels pore was identified as Val793, Leu794, Phe797, and Cys759 in domain I/S6, and Ile1279 in domain II/S6. Our findings imply that CBD favorably binds to the $Na_v1.4$ channel in its slow-inactivated state.

Keywords: cannabidiol; $Na_v1.4$ channel; myotonia; fast inactivation; slow-inactivation

Citation: Huang, C.-W.; Lin, P.-C.; Chen, J.-L.; Lee, M.-J. Cannabidiol Selectively Binds to the Voltage-Gated Sodium Channel $Na_v1.4$ in Its Slow-Inactivated State and Inhibits Sodium Current. *Biomedicines* **2021**, *9*, 1141. https://doi.org/10.3390/biomedicines9091141

Academic Editor: David R. Wallace

Received: 16 August 2021
Accepted: 1 September 2021
Published: 2 September 2021

1. Introduction

The voltage-gated sodium channel is a hetero-multimeric protein composed of a large ion-conducting, voltage-sensing α-subunit and a few smaller β-subunits [1–5]. The voltage-gated sodium channel $Na_v1.4$ of the skeletal muscle is a heterodimer consisting of a pore-forming α and a regulatory β1-4 subunit [6,7]. The α-subunit contains four homologous domains (DI–DIV), each with six transmembrane segments [6,7]. During depolarization, the S4 segments in each domain, containing positive amino acid residues and functioning as voltage sensors, can move outward to alter the channel conformation and modify its biophysical property [1–7]. The different charge residues of the S4 segments play an important role in determining domain-specific functions [6,7]. The S4 segments in the domains DI and DII are thought to be key molecules for the activation of the sodium channel, whereas the S4s in DIII and DIV regulate the fast inactivation process. The pore with its selectivity filter is lined by the loops formed between the S5 and S6 segments of each domain [1–5]. It has been reported that the pore of the $Na_v1.4$ channel can be an interaction site for pharmacological blockers, such as lidocaine, benzocaine, and

ranolazine [8,9]. The pore exhibits four intra-bilayer fenestrations, connecting it with the bilayer core. Nevertheless, their functional role remains elusive [10].

Most of the skeletal muscle channelopathies arise from *de novo* or autosomal dominant mutations in the *SCN4A* gene, which encodes the α-subunit of the $Na_v1.4$ channel [11–14]. The mutations in the $Na_v1.4$ channel result in alterations of skeletal muscle excitability [15–17]. Non-dystrophic myotonia with increased excitability of the muscle membrane, such as myotonia congenita (MC) and paramyotonia congenita (PMC), are the primary clinical phenotypes [15,17]. The gain-of-function mutations in MC and PMC enhance inward Na^+ currents, leading to an impairment of activation with a hyperpolarized shift [11,15,18–20]. The study of these disorders has provided insights into the structure–function relationship of the sodium channel and rational approaches for therapeutic intervention in many disorders associated with cellular hyperexcitability [21]. Hyperexcitable muscle channelopathies with mutations in the $Na_v1.4$ channel have been classified into non-dystrophic myotonia and periodic paralyzes [11,20]. Electrophysiological studies in a heterologous expression system with $Na_v1.4$ mutations have shown variable biophysical defects in activation, fast inactivation, and slow-inactivation [22,23]. The mutations could lead to an initial myotonia discharge burst and result in stiffness and weakness in affected patients [24,25].

Recently, cannabidiol (CBD) was reported to be a potentially beneficial compound to treat epilepsy in children [26,27]. CBD is one of the 113 identified cannabinoids extracted from the cannabis plant [28]. Trials using CBD to treat a few disease entities such as anxiety, cognition decline, movement disorders, and pain have been conducted, although high-quality evidences to prove the effectiveness have not yet been obtained [29,30]. In addition, the CBD-enriched hemp oil was found to have the anti-cancer property with increasing of oxidative stress [31]. There are a few routes of CBD ingestion, it can be taken directly by mouth, the cannabis smoke can be inhaled by nose, or the aerosol spray of CBD can be absorbed by the cheek mucosa [32,33].

Moreover, CBD was suggested to be a potentially therapeutic compound against a variety of conditions, such as muscle spasms, pain, and myotonia [11]. Some reports of CBD's efficacy are anecdotal, whereas others were experimentally and clinically substantiated [34–36]. CBD showed therapeutic efficacy against Dravet and Lennox Gastaut syndromes in clinical trials phase III [11,34–36]. The efficacious dosage against the Dravet syndrome is around 20 mg/kg [35]. However, the mechanism underlying CDB efficacy and its associated biophysical changes on channelopathies remain elusive. Considering the lack of therapy for myotonia resulting from $Na_v1.4$ channel mutations, we investigated whether CBD could represent another drug of choice for the treatment of symptoms.

Our results suggest that CBD can selectively bind to the $Na_v1.4$ channel in its inactivated state with a dissociated constant of approximately 31.5 μM. Moreover, the binding affinity for the fast-inactivated state was four times lower than that for the slow-inactivated one. CBD exhibited significantly higher binding kinetics to the slow—compared to the fast—inactivated $Na_v1.4$ channels. Using the molecular docking model, we identified five CBD binding sites at the bundle crossing region in the $Na_v1.4$ channel pore, which may affect conformational changes in the slow-inactivated gate. These results suggest that CBD could serve as a distinct therapeutic drug for $Na_v1.4$ channelopathies.

2. Experimental Section

2.1. Wild-Type (WT) $Na_v1.4$ Channel CDNA Constructs

The cDNA clone with the *SCN4A* gene, which encodes the α-subunit of sodium channel $Na_v1.4$, was obtained from OriGenes Technologies Company (Cat. No. RC218290; Rockville, MD, USA). The SCN4A cDNA was seamlessly cloned into the mammalian expression cloning vector pcDNA3.1(+)-DYK vector [37,38].

2.2. Transient Transfection of Chinese Hamster Ovary (CHO-K1) Cells

The cells were grown and incubated under the culture condition as in our previous study [37,38]. Briefly, CHO-K1 cells were incubated in the F12K medium (Thermo Fisher Scientific, Waltham, MA, USA) with 5% CO_2 at 37 °C, supplemented with 10% fetal bovine serum (Thermo Fisher Scientific) and 0.2% Normocin (InvivoGen, San Diego, CA, USA). The cells with a density of 1.0×10^6 were seeded onto a 3.5 cm culture dish (Greenpia Technology, Seoul, South Korea). Transient transfection was carried out using the Lipofectamine™ 3000 reagent (Thermo Fisher Scientific). After 24 h of transfection, the cells were washed with the F12K medium. Then, the CHO-K1 cells stayed in culture for 96 h until the electrophysiological experiments.

2.3. Whole-Cell Patch-Clamp Recording

Before the whole-cell patch-clamp recording, the proteinases IIX-III (0.025 mg/mL; Sigma–Aldrich, St. Louis, MO, USA) were added to the transfected cells. CHO-K1 cells with the expressed $Na_v1.4$ channel were plated onto 1.2 cm coverslips (Paul Marienfeld GmbH, Lauda-Königshofen, Germany) at 37 °C for approximately 45 min. Whole-cell patch-clamp recordings were carried out within four days of transfection. Currents were recorded using an Axopatch 700B amplifier at 25 °C (Axon Instruments, Sunnyvale, CA, USA), interfaced with the pClamp 9.2 acquisition software (Molecular Devices, San Jose, CA, USA). Currents were filtered at 5 kHz with a four-pore Bessel filter and digitized at 50 μs intervals using a signal conditioning amplifier, the Digidata-1322A interface (Axon Instruments, Union City, CA, USA). For patch-clamp recording, fire-polished, borosilicate glass-pulled micropipettes were prepared using a Sutter P-97 puller (Sutter Instrument Company, Novato, CA, USA). The pipette resistance was 1.5–2.5 mΩ. The glass electrode pipette was filled with an internal solution containing the following (in mm): 75 CsCl, 75 CsF, 5 HEPES, 2 $CaCl_2$, and 2.5 EGTA (pH 7.6). The whole-cell configuration was immersed in the external solution which contains the following ingredient (mm): 150 NaCl, 10 HEPES, 2 $CaCl_2$, and 2.5 $MgCl_2$ (pH 7.6). Electrophysiological recording started approximately 5 min after establishment of a whole-cell configuration, which allowed reaching an equilibrium with internal solution in the intracellular compartment at the imposed holding membrane voltage (especially at −120 mV).

2.4. Chemical Drugs

CBD was purchased from Sigma–Aldrich (Burlington, MA, USA). CBD was dissolved in methanol to a stock concentration of approximately 31.8 mm. After being aliquoted, it was stored at −20 °C. A fresh aliquot of the drug was used for each experiment, which was diluted with an external solution to reach the required concentration.

2.5. Molecular Docking of CBD to the $Na_v1.4$ Channel

The CDOCKER program in the DS 2020 software (BIOVIA, Dassault Systems, Discovery Studio, 2020, San Diego, CA, USA) was employed to model the CBD docking to the human $Na_v1.4$ channel. The molecular mimicry screened for the CBD binding site potential in the human $Na_v1.4$ channel [39]. The X-ray diffraction structure of the human $Na_v1.4$ channel in complex with the β-subunit was downloaded from the Protein Data Bank (PDB ID: 6GAF; https://www.ncbi.org/) (19 October 2018) [10]. Ligands were prepared to obtain adequate biological ionization and tautomerization status. The central domain of the human $Na_v1.4$ channel was defined as the binding pocket. The model yielded the 10 best binding poses of CBD, ranked by the mean energy score. CDOCKER energy values of CBD with the human $Na_v1.4$ channel were obtained as standard to select good predictions of affinity peptides (calculated in kcal/mol).

2.6. Data Analysis

All electrophysiological sweeps were analyzed using the software Clampfit 9.0 (Axon Instrument, San Jose, CA, USA). Steady-state inactivation curves were fit to a Boltzmann

function to obtain the midpoint (V_h) and slope (k) values. Time constants for recovery were obtained by fitting data from each cell to a first-order exponential function and the averaging time constants across cells. Statistical data were analyzed using Sigmaplot software 10.0 (Systat Software Inc, Chicago, IL, USA) and are described as means ± standard error of the mean. Data were assessed and analyzed using Student's independent t-tests, and statistical significance was defined as $p < 0.05$.

3. Results

3.1. The Assessment of Transient Sodium Current Inhibition by CBD with Variable Holding Potentials on the CHO Cells Expressing $Na_v1.4$ Channel

We first assessed possible changes in $Na_v1.4$ channel activation after the binding of CBD. We demonstrated a negligible inhibitory effect in the activation of transient $Na_v1.4$ currents in CHO-K1 cells held at −120 mV upon treatment with different concentrations (between 3 and 100 μM) of CBD (left panel of Figure 1A). However, the inhibitory effect of CBD escalated in a dose-dependent manner, while the holding potentials increased from −120 to −80 mV (Figure 1A). To confirm the influence of holding potential on the inhibitory effect of CBD, the CHO-K1 cells were next subjected to a holding potential between −70 and −120 mV, and the inhibition of sodium currents was evaluated with different concentrations of CBD (3, 10, 30, to 100 μM; Figure 1B). Compared to the depolarization currents in the control condition (no CBD), there was a significant decrease in relative currents along with the increased concentration of CBD. Moreover, the inhibitory effect was found to be enhanced with the escalation of holding potential (from −120 to −70 mV; Figure 1B). Each of the data could be well fitted by the one-to-one binding curve, which provides a rough estimate of apparent dissociation constants (K_{app}) of 1341.7, 275.5, 96.9, 30.1, 10.1, and 4.1 μM for CBD binding at the holding potentials of −120, −110, −100, −90, −80, and −70 mV, respectively. The holding potential-dependent K_{app} value also reduced with escalation of the holding potential (Figure 1B). The suppression was significant at −80 mV and even more pronounced at −70 mV. Cells holding at −120 mV were nearly devoid of suppression, with only a "closed"-state $Na_v1.4$ channel available. The stronger membrane depolarization was, the more abundant were the inactivated channels. These findings indicate that CBD presumably binds more favorably to the inactivated than to the resting channels. Moreover, the K_{app} values from 1341 to 4.1 μM at different holding potentials did not show a monotonous or commensurate trend of alteration along with the different concentrations of CBD, which implies that at different holding potentials, CBD binds to a mixture of variable gating states of $Na_v1.4$ channels.

3.2. The Influence of CBD on the Inactivated Curve of $Na_v1.4$ Channels Following a Short Depolarizing Pulse

Previous studies on the gating properties of sodium channels have demonstrated their conversion from open, inactivated states to closed states [40]. The inactivated channels can be obtained and classified into fast and slow-inactivation according to their period of depolarization [41]. To discern to which of the inactivated channel states CBD was preferentially bound, we examined the influence of CBD on the inactivated curve of $Na_v1.4$ channels following a short depolarizing pulse (approximately 100 ms). For the fast-inactivating state, a series of depolarization prepulses, which escalated from −120 to −20 mV for 100 ms, were applied to the CHO-K1 cells, followed by a test pulse at 0 mV for 3 ms (left panel of Figure 2A). The sweep traces were recorded in both the control and CBS treatment (30 μM) conditions (right panel of Figure 2A). We defined "fraction available" as the recovered channels from fast inactivation. Then, the inactivation curve was depicted using the "fraction available" against the depolarizing membrane potential, between −120 and −20 mV (Figure 2B). The fast inactivation curve showed no significant shift upon treatment with 30–100 μM of CBD, as compared to controls (Figure 2B). Furthermore, the inactivation curve of those channels after washing out of the CBD did not show a significant deviation from the control and CBD treatment conditions (Figure 2C). Figure 2D shows no significant change in depolarizing membrane potential (ΔV) in those with 30 μM of

CBD and those after washing out of CBD. The ΔV was defined as the relative depolarizing membrane potential at which 50% of the channels were available (50% of fraction available), compared to the controls. Similarly, there was no significant change in the slope factor for the inactivation curves (Figure 2D). These data indicate that steady-state occupancy of the $Na_v1.4$ channel binding sites by CBD was rarely achieved in accordance with the short depolarization (fast inactivation) pulse.

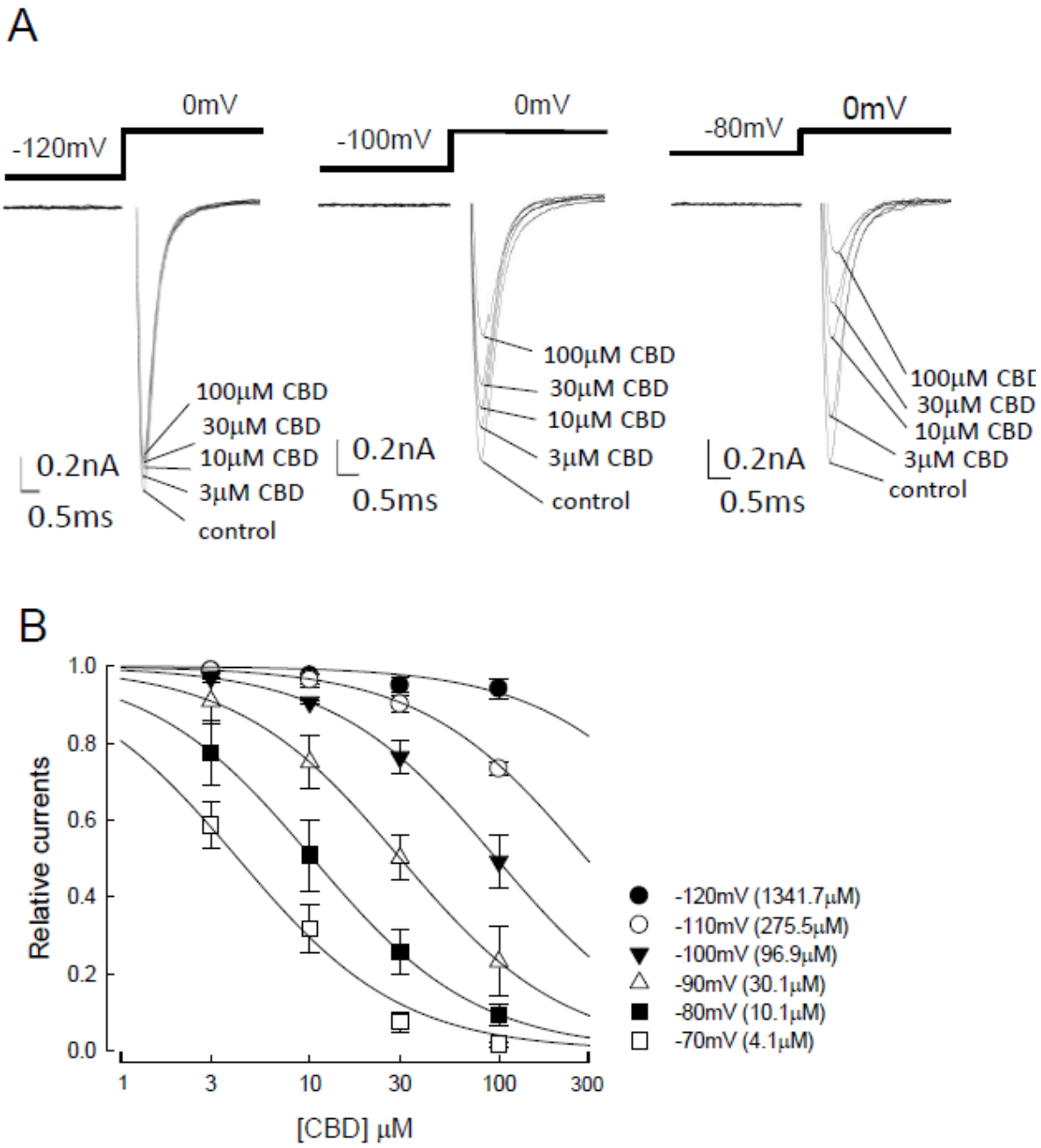

Figure 1. Inhibition of the activation of $Na_v1.4$ sodium channel by cannabidiol at different holding potentials. (**A**) Current traces of the patched cells expressing $Na_v1.4$ channels were recorded under treatment with different concentrations (0, 3, 10, 30, and 100 μM) of cannabidiol (CBD). The cells were held at −120, −100, and −80 mV, followed by depolarization to 0 mV for 5 ms. (**B**) Dose–response curves for inhibition of $Na_v1.4$ sodium currents by CBD at different holding voltages between −120 and −70 mV (n = 5 for a low to high concentration of CBD). Peak currents in the presence of CBD were normalized to control peak currents at each of the different holding potentials and plotted against the CBD concentration. Lines are the fits of data using the following formula: relative current = $1/[1 + ([CBD]/K_{app})]$, where [CBD] was the CBD concentrations and K_{app} values were 1341.7, 275.5, 96.9, 30.1, 10.1, and 4.1 μM at the holding potentials of −120, −110, −100, −90, −80, and −70 mV, respectively.

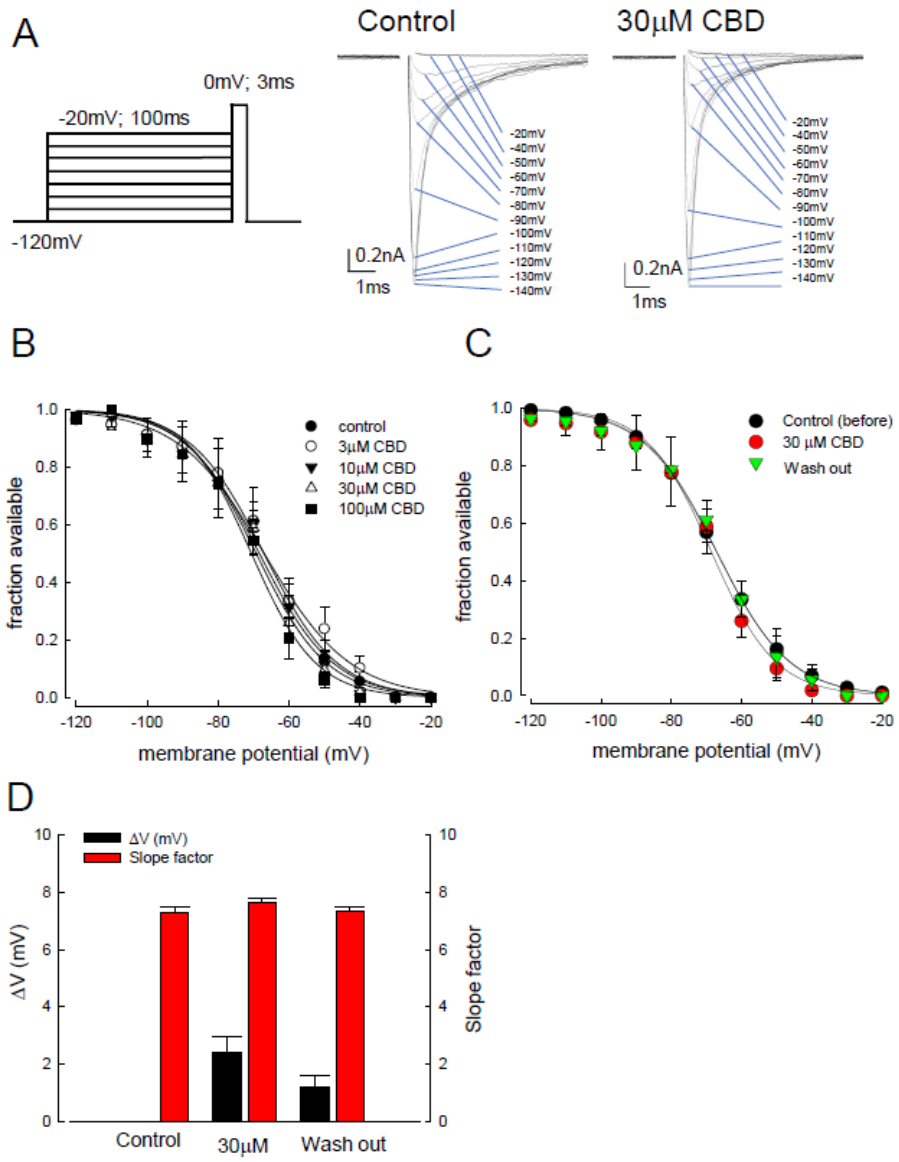

Figure 2. Cannabidiol induced changes in the fast inactivation curve of $Na_v1.4$ channel. (**A**) In our electric protocol to test the fast inactivation of $Na_v1.4$ channels, the cell was held at −120 mV and then stepped to the depolarizing pulse up to −20 mV (in 10 mV steps) for 100 ms, followed by a test pulse, 0 mV for 3 ms (left panel). The representative current sweeps of the $Na_v1.4$ channel was recorded after the short test pulse (right panel). (**B**) The inactivation curve shifted by CBD from the cells expressing $Na_v1.4$ channel is shown. Fraction available, defined as the normalized peak current (to the peak current with an inactivating pulse at −120 mV), is plotted against the voltage of the inactivating pulse, between −120 and −20 mV, to show the inactivating curve. The inactivating curve did not shift significantly under treatment with different CBD concentrations (3, 10, 30, or 100 μM CBD). (**C**) The inactivation curves of the control, CBD treatment, and washing out channels demonstrate no significant voltage shift during the approximately 100 ms depolarizing pulse. Lines are best fit using the Boltzmann function $1/(1 + \exp[(V - V_h)]/k)$, where V_h were −67.1, −71.7, and −67.4 mV, and k values were −10.4, −9.8, and −10.7 for control, those cells after treatment of 30 μM CBD, and those with washing out, respectively. (**D**) The shifts in inactivation curves (ΔV_h) in Figure 2C were 1.8 and 1.5 mV for those cells with 30 μM of CBD and those after washing out, respectively. The k values were 7.3 ± 0.1, 7.6 ± 0.2, and 7.3 ± 0.2 for control, those cells with 30 μM of CBD, and those post washing out of CBD, respectively (n = 5).

3.3. Exploration of Whether CBD Can Bind to the Slow-Inactivated $Na_v1.4$ Channel with an Elongation of the Depolarizing Prepulse

To explore whether CBD can bind to the slow-inactivated $Na_v1.4$ channel, a new protocol with elongation of the depolarizing prepulse up to 18 s was designed (Figure 3A). The sweep traces at different depolarizing potentials were recorded in the control and CBD treatment (30 μM) conditions (Figure 3A). After treatment, the activation curve was inhibited as compared to the controls. The different concentrations of 3, 10, 30, and 100 μM of CBD were applied to the CHO-K1 cells, and then the availability of sodium channel (fraction available) against the escalating depolarizing prepulse potentials from −120 to −40 mV was depicted in those cells with the treatment of CBD (Figure 3B). The curve was significantly left-shifted along with the increase of CBD concentration in a dose-dependent manner. Moreover, such a shift was reversed to the original state when CBD was washed out (Figure 3C). The prominent shift of the curve suggests a variable binding affinity between CBD and the different gate states of $Na_v1.4$ channels. The slope factors for the curve at different concentrations of CBD were not different from those of the controls (Figure 3D). Nevertheless, a significant increase in ΔV (the differential membrane potential between the controls and those cells with CBD treatment at 50% fraction available) was observed after treatment, in a dose-dependent manner (Figure 3E). The hyperpolarizing shift (left shift) indicates the inactivation occurs at a lower membrane potential than the controls. The larger the value of ΔV, the more efficient it is for the channel to evolve into an inactivated state. Thus, if CBD binds to the inactivated state of the Na_v14 channel, a higher concentration of CBD would render a larger value of ΔV. According to the inactivation curve shifts (ΔV) with different concentrations of CBD, the deduced K_d was approximately 1.2 μM (Figure 3F) [41–43]. The 18 s of inactivating pulse can not only allow more time for CBD binding but also distributes the channel to different gating states beyond its fast inactivation. These findings suggest that CBD can bind to the slow-inactivated $Na_v1.4$ channel after the application of variable depolarization voltages.

3.4. Determination of $Na_v1.4$ Channel Slow Inactivated State

To evaluate the slow-inactivation of the $Na_v1.4$ channel, another approach resulting in more accurate measurement was next employed. The protocol was designed as follows. After a depolarization at 0 mV for 20 ms, the time for resting membrane potential, −120 mV was prolonged successively until the next test potential, 0 mV for 20 ms (Figure 4A). Most of the inactivated $Na_v1.4$ channels could recover within approximately 30 ms at −120 mV (right panel of the Figure 4A). Based on the findings, we assumed that the contribution of the available channels after fast inactivation can be minimized when the time laps was protracted longer than 30 ms. We then evaluated whether the voltage of depolarized membrane potential and the periods of the activation time (30 ms) influenced the slow-inactivation. With two different depolarizing potentials, −80 (Figure 4B) and −10 mV (Figure 4C), the relative currents that represented the available channels after slow-inactivation were evaluated. Less than 10% of the $Na_v1.4$ channels entered the slow-inactivated state with a membrane potential of −80 mV in 14 s (Figure 4B), whereas approximately 90% of the $Na_v1.4$ channels entered the slow-inactivated state at −10 mV (with a time constant of approximately 1.5 s, Figure 4C). Finally, we assessed the difference in the transient inactivation and the slow-inactivation curves of the $Na_v1.4$ channel. To depict the slow-inactivation curve, the depolarizing membrane potential was −10 mV for 30 s and then repolarized in a 20 ms gap followed by a test pulse at 0 mV for 10 ms. The slow-inactivation curve showed a depolarizing shift compared to the fast inactivation curve (right panel of Figure 4D).

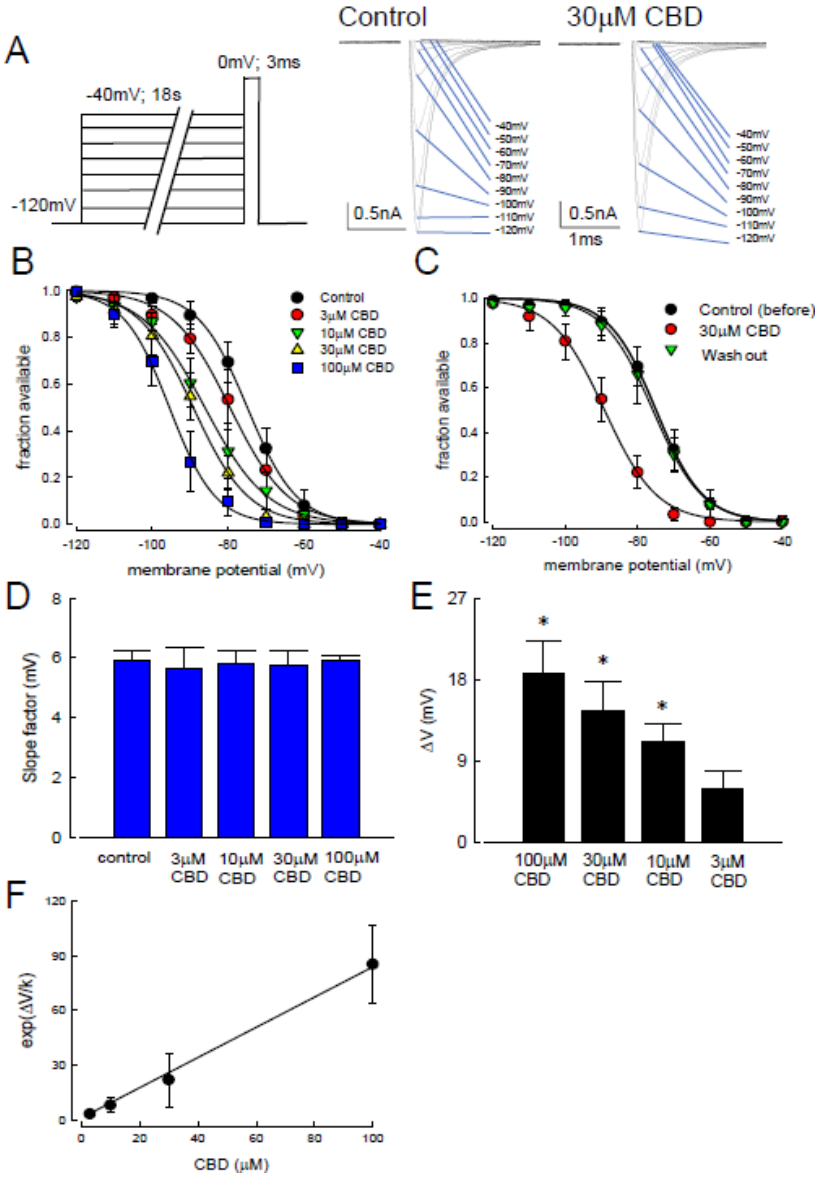

Figure 3. Changes in the slow-inactivating curve after the applications of cannabidiol. (**A**) The experiment protocols were similar to those of Figure 2, however, the duration of inactivation pulse was protracted to 18 s (left panel). The representative current sweeps for slow-inactivation of $Na_v1.4$ in the control channels and those treated with 30 μM of CBD were recorded after the short test pulse (right panel). (**B**) The inactivating curve was shifted left in a dose-dependent manner after treatment with different concentrations of CBD. No significant change in slope was found in these curves. Lines of best fit were fitted using the Boltzmann function $1/(1 + \exp[(V - V_h)]/k)$, where V_h were -74.9 ± 0.4, -79.5 ± 0.6, -83.1 ± 0.5, -89.2 ± 0.6, and -95.5 ± 0.4 mV, and k values were -6.5 ± 0.3, -7.6 ± 0.5, -8.4 ± 0.4, -7.2 ± 0.4, and -6.0 ± 0.3 for the control channels and those channels treated with 3, 10, 30, and 100 μM of CBD, respectively. (**C**) The inactivation curves in the control channels, those treated with 30 μM of CBD, and those after washing out. There was a hyperpolarized shift of the inactivation curve in those channels upon treatment with 30 μM of CBD. Lines are fit using the Boltzmann function $1/(1 + \exp[(V - V_h)]/k)$, where V_h were -7.4 ± 0.4, -89.2 ± 0.6, and -75.9 ± 0.5 mV, and k values were -6.5 ± 0.3, -7.2 ± 0.45, and -6.8 ± 0.37 for the control channels, those with 30 μM CBD, and the washing out channels, respectively. (**D**) CBD did not significantly change the slope factor k. Cumulative results showed that the average values in the control channels and those channels after treatment with 3, 10, 30, and 100 μM of CBD were 5.8 ± 0.3, 5.6 ± 0.7, 5.8 ± 0.4, 5.7 ± 0.5, and 5.9 ± 0.1, respectively. (**E**) A dose-dependent shift in V_h for the inactivation curve. Comparing to the controls, the degree of voltage shift was 5.9 ± 1.9, 11.1 ± 1.9, 14.5 ± 3.3, and 18.7 ± 3.6 mV for those channels after treatment with 3, 10, 30, and 100 μM of CBD, respectively, (*, $p < 0.05$). (**F**) The exp(ΔV/k) values are plotted against the concentration of CBD. ΔV/k were derived from mean values Figure 3D,E. The line is a best fit to the data of the formula exp(ΔV/k) = 1 + ([CBD]/1.3), where the y-intercept is 1. The [CBD] denotes the CBD concentration in μM [42–44].

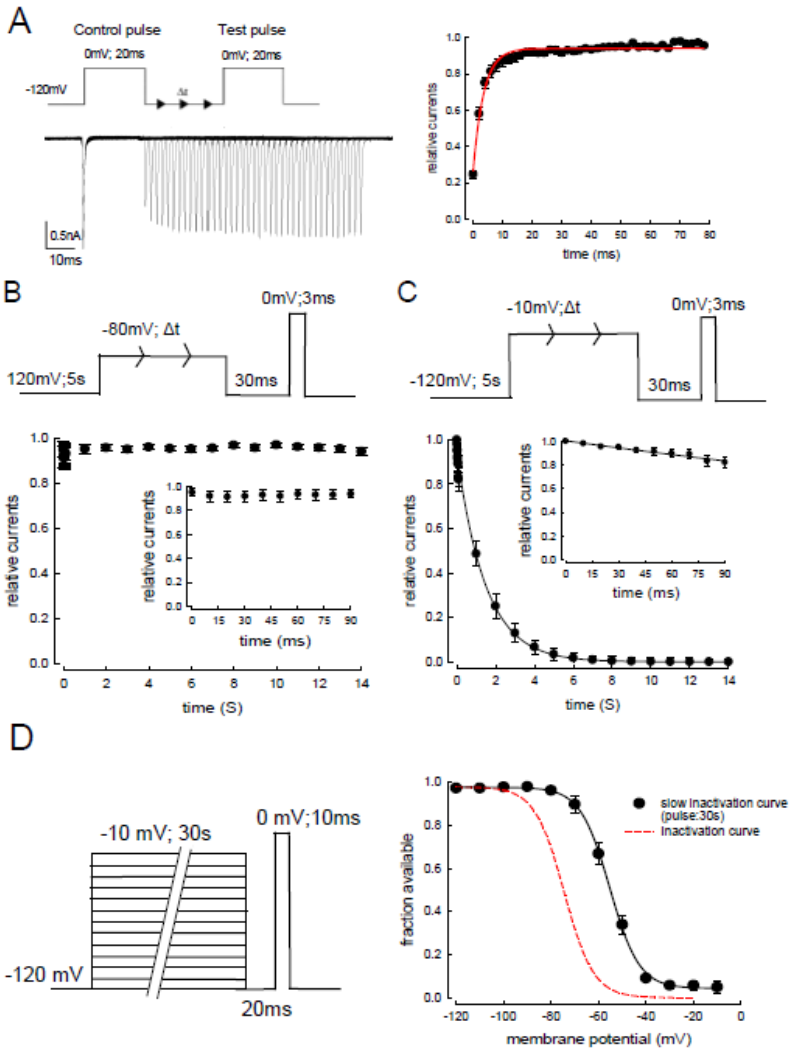

Figure 4. Recovery course from the fast and slow-inactivation curves in $Na_v1.4$ channels. (**A**) The cell was held at −120 mV and pulsed twice to 0 mV (for 20 ms each) every 2 s, with a gradually lengthened gap between the two pulses at −120 mV. Sweeps were arranged so that the currents in the second pulse gradually shifted rightward as the gap lengthened (by 1 ms each sweep, left panel). The relative current, defined as the normalized peak current in the second pulse to that in the first pulse, is plotted against the duration of the intervening gap (n = 5, right panel). The plot shows that most channels entering the fast inactivation recovered after approximately 20 ms at −120 mV. (**B**) The electric protocol to evaluate the kinetics of slow-inactivation at −80 mV. The patch CHO-K1 cell was held at −120 mV for approximately 5 s, followed by a depolarized pulse −80 mV for a certain time. Then, the current of −120 mV for 30 ms was applied to the cell to allow full recovery from the fast inactivation. A test pulse at 0 mV for 3 ms was employed to evaluate the slow-inactivation. The elicited currents were normalized to the control current, relative currents, which was then plotted against the duration of the inactivating pulse at −80 mV (time in seconds). The inset figure is a close-up view of the first 90 ms of data. Most (>90%) of the $Na_v1.4$ channels remained in the fast-inactivated state at −80 mV. (**C**) The electric protocol to evaluate the kinetics of slow-inactivation at −10 mV. The same protocols and analyses were employed as shown in Figure 4B, except that the inactivating pulse was set to −10 mV (n = 5). In this case, most $Na_v1.4$ channels (>90%) entered the slow-inactivated state with a time constant of 1.43 s from the exponential fit to these points. (**D**) The patched cell was held at −120 mV, and the pulse protocol was repeated every 30 s. Depolarizing prepulses of varying voltages from −120 to −10 mV (approximately 30 s) were applied to the cells, followed by a gap voltage at −120 mV for 20 ms to allow recovery from fast inactivation. Subsequently, a test pulse at 0 mV for 10 ms was applied to evaluate the fraction of available channels. The curve was fitted using the Boltzmann function $1/1 + \exp[(V - V_h)/k]$, where the V_h value was -54.9 ± 0.7 mV and the k value was -7.3 ± 0.5 (the black curve, right panel). The left of the inactivation curve from Figure 3B is replotted with a dashed line on the voltage axis.

3.5. Evaluation of Different Depolarizing Potentials Influence on the CBD Inhibitory Effect

To further confirm that CBD can bind to the $Na_v1.4$ channel in its slow-inactivation state, the channel was depolarized to −10 or −80 mV for 18 s with the treatment of different concentrations of CBD (Figure 5A,B). The available $Na_v1.4$ channels were assessed by the period of time (Δt) at −120 mV, evaluating the relative currents after prolonged depolarization with a subsequent certain period of repolarization. During the period, the $Na_v1.4$ channels were supposed to be recovered from the inactivated state, evolving to a closed state, which can then be activated by the test pulse. Thus, the relative currents represented the channels recovered from the inactivated state. Since the period is scaled in seconds, we assumed that only the slow-inactivated state $Na_v1.4$ channels were available. Furthermore, the relative currents recorded from CHO-K1 cells under the treatment of different concentrations of CBD were the indices for the binding of CBD to the slow-inactivated $Na_v1.4$ channels. The larger the relative current was, the more channels were available, which indicates a more efficient dissociation of the complex of CBD/slow-inactivated $Na_v1.4$ channels (Figure 5A,B). As time (Δt) elapsed, the relative current increased quickly and attained ~90% of the controls (Figure 5A,B). With the treatment of CBD, there was a decremental change in the relative currents in a dose-dependent manner (Figure 5A,B). The slowing of the recovery kinetics was embodied by the decrease in the area under the recovery time course (Supplementary Data Figure S1), which was already manifested by the cells treated with 3–10 μM of CBD at a depolarized pulse of −10 mV (Figure 5A,B). The effect was saturating with 100–300 μM of CBD, which was well described by a one-to-one binding curve with a K_d to the slow-inactivated state of the $Na_v1.4$ channel at approximately 31.5 μM (Figure 5C). Since the slow-inactivated state is the dominant one after strongly depolarizing the membrane potential for such a long time, we postulated that CBD selectively binds to the slow-inactivated $Na_v1.4$ channels with a K_d of approximately 31.5 μM. In contrast, a similar approach with an activating pulse of −80 mV for 18 s resulted in a K_d of 127.3 μM (Figure 5D) [41]. Since the depolarizing potential at −80 mV may not provide adequate available slow-inactivating channels, the value of K_d was much larger than for the channels with prepulse depolarization at −10 mV (approximately 31.5 μM). We therefore conclude that CBD can selectively bind to the slow-inactivated channel.

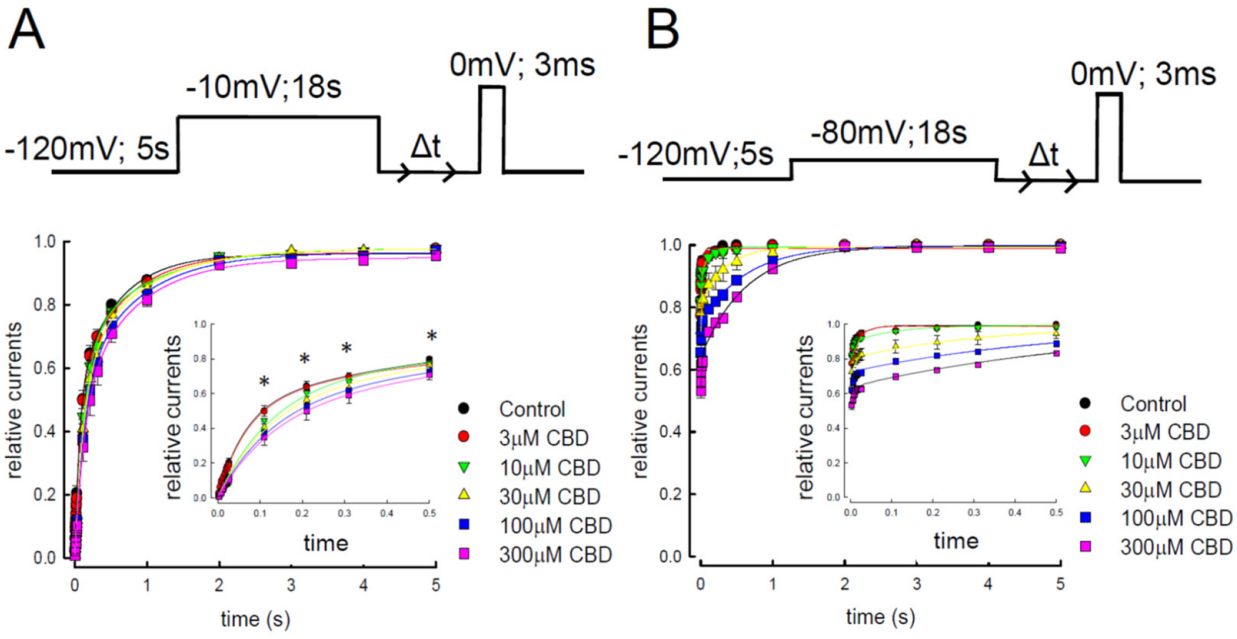

Figure 5. *Cont.*

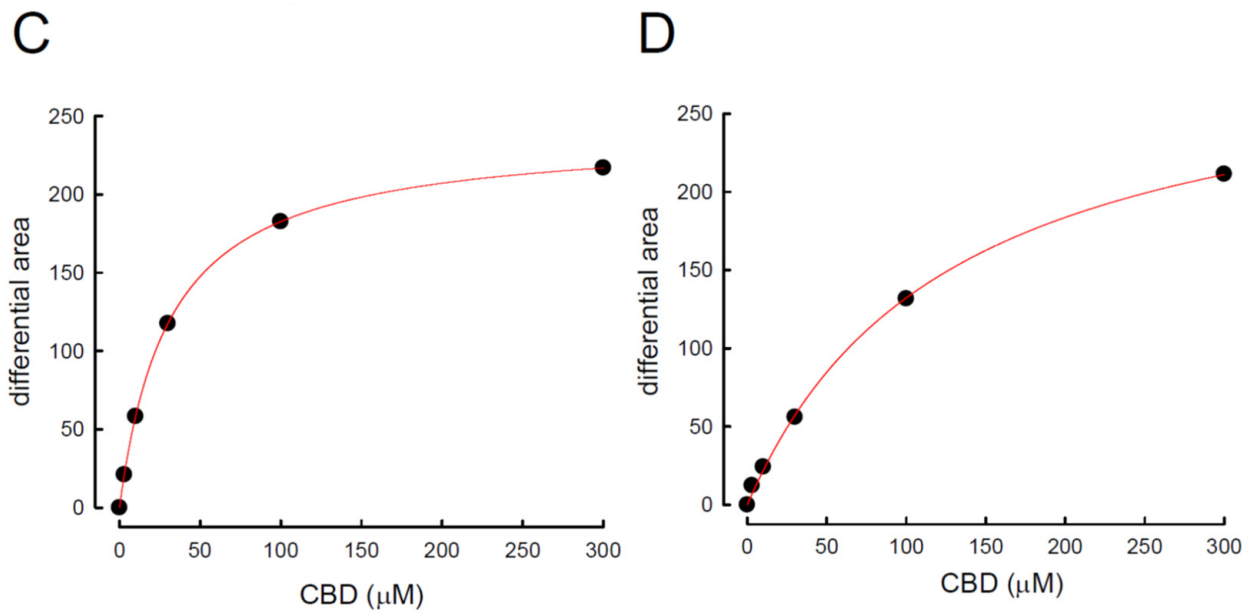

Figure 5. Recovery course from slow-inactivation and affinity of cannabidiol to the slow-inactivated $Na_v1.4$ channel. (**A**) Patched cells expressing the $Na_v1.4$ channel were held at −120 mV for 5 s. An inactivating pulse at −10 mV for 18 s was applied with a subsequent repolarization to −120 mV for a certain time to eliminate the channels with fast inactivation. The second test pulse of 0 mV was applied after an intervening gap at −120 mV for different lengths of time (0.003, 0.006, 0.009, 0.012, 0.015, 0.018, 0.021, 0.024, 0.027, 0.11, 0.12, 0.31, 0.51, 1, 2, 3, 4, and 5 s). Representative currents were overlaid according to the time sequence of examination. Time scales were applied for current kinetics only. The relative current, defined as the normalized peak current in the second test pulse (to the peak current in the first test pulse), was plotted against the length of intervening gap to obtain the time course of recovery from slow-inactivation in control (n = 5) $Na_v1.4$ channels and those treated with different concentrations of CBD (n = 5). Note the close-up view of the first 500 ms of data shows a significant dose-dependent change in the recovery of slow-inactivation after CBD treatment (inset figure is a closed-up view of Figure 5A; * $p < 0.05$). (**B**) Approaches and analysis protocols were the same as in Figure 5A, except that the inactivating pulse was set at −80 mV for 18 s. (**C**) Difference between the area in control and upon different concentrations of CBD in Figure 5A to the maximal difference giving the relative difference in the area, which is plotted against the CBD concentration (see Supplementary Data Figure S1). The line is the fit of data points using the following formula: relative difference in area = ([CBD]/31.5)/(1 + [CBD]/31.5), where [CBD] denotes CBD concentration in μM [41]. (**D**) Analysis protocols were the same as those of Figure 5B, except that the inactivating pulse was set at −80 mV for 18 s. The line is the fit using the following formula: relative difference in the area = ([CBD]/127.3)/(1 + [CBD]/127.3), where [CBD] denotes CBD concentration in μM [41].

3.6. Evaluation of CBD Inhibition by the Time Elapse for Depolarization in $Na_v1.4$ Channel

To further investigate the binding kinetics between $Na_v1.4$ channels and CBD, the protocol illustrated in Figure 6A was designed. The $Na_v1.4$ channels were depolarized at −10 mV for a variable of time period (Δt), which allowed the binding between CBD (3–100 μM) and the $Na_v1.4$ channels. After a period of repolarization, −120 mV for 200 ms to eliminate the fast-inactivated $Na_v1.4$ channels, a test pulse was applied to obtain the current that represented the available $Na_v1.4$ channels recovered from the slow-inactivation. As shown in the lower panel of Figure 6A, the higher the concentration of CBD was, the less sodium current was obtained. The differential currents, defined as the currents from CHO-K1 cells treated with CBD at a certain time of depolarization relative to the controls, increased in a dose-dependent manner (Figure 6B). The kinetics of current decreases were found to be linearly correlated to CBD concentrations, giving a binding rate constant of approximately 64,000 M^{-1} s^{-1} (K_{on}) with the treatment of 3–100 μM (Figure 6C, solid line). The unbinding rate, or the y-intercept, of the linear fit to the fastest macroscopic binding rate (i.e., approximately 64,000 M^{-1} s^{-1}) in Figure 6C, was approximately 0.7 s^{-1} (K_{off}). These kinetic data thus implicate a dissociation constant ($K_d = K_{off}/K_{on}$) of approximately

10.7 μM. These findings suggest that CBD favors binding to the $Na_v1.4$ channel in its slow-inactivated state.

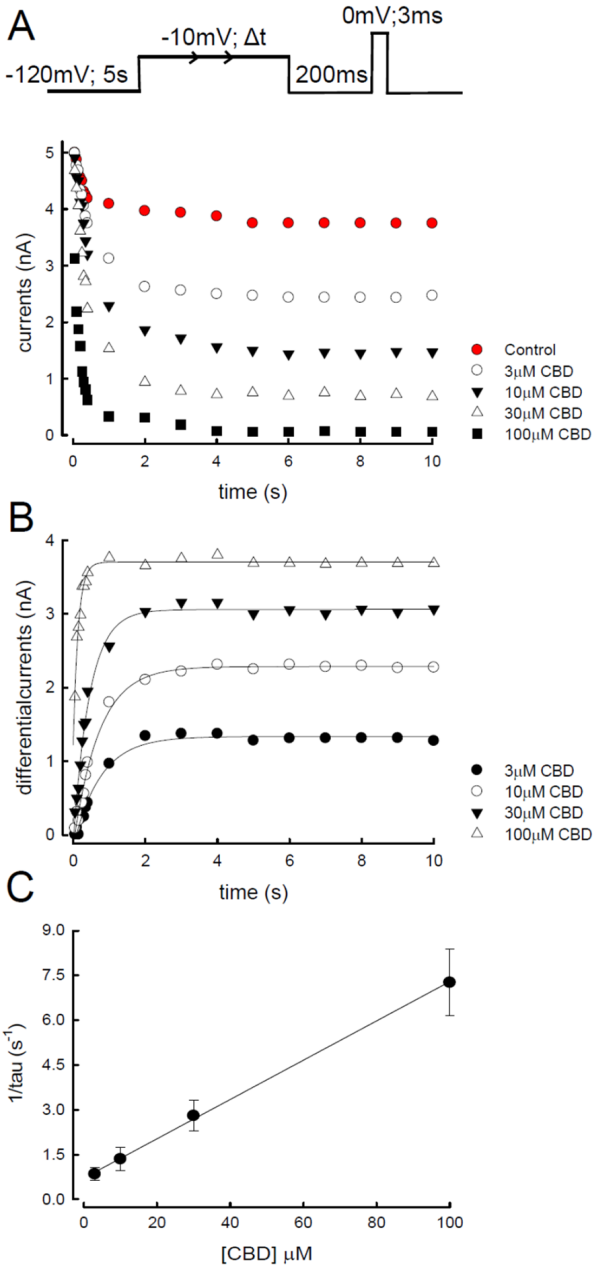

Figure 6. Binding rate of cannabidiol to the slow-inactivated $Na_v1.4$ channel. (**A**) Patched cells were held at −120 mV for 5 s and stepped to an inactivating pulse at −10 mV for various durations of time (0.05, 0.1, 0.15, 0.2, 0.25, 0.3, 0.35, 0.4, 1, 2, 4, 5, 6, 7, 8, 9, and 10 s). The cells were then subjected to a fixed gap at −120 mV for 200 ms, which was set to allow for partial recovery of the slow-inactivated channels to obtain measurable currents elicited by the subsequent test pulse at 0 mV. Elicited currents were plotted against the duration of the inactivating pulse (−10 mV), and the representative currents were overlaid according to the time sequence. (**B**) Differential currents between the CBD and control conditions. Data were obtained from Figure 6A and are plotted against the duration of the prepulse. The time constants from the fit were 801.3, 740.2, 454.5, and 138.7 ms for the different CBD concentrations, namely, 3, 10, 30, and 100 μM, respectively. (**C**) The reciprocal of the time constant from that fitted in Figure 6B is plotted against the concentrations of CBD. The slope of the solid line is 64,000 M^{-1} s^{-1}, and the y-intercept is 0.7 s^{-1}.

3.7. Molecular Mechanism of the $Na_v1.4$ Channel with Cannabidiol

To inspect the CBD binding site on the $Na_v1.4$ channel, the molecular docking model was used (Figure 7A,B) [39]. The binding sites of CBD were found to be close to domains I (green) and II (dark red) of the $Na_v1.4$ channel (Figure 7C,D). The binding of domain I (DI/S6) to CBD stabilized four conventional π alkyl interactions with the residues C759, V793, L794, and F797 at the gating hinge of the bundle crossing region of DI/S6 in the $Na_v1.4$ channel pore (Figure 7E). Moreover, the atom of CBD also formed one conventional π alkyl interaction with residue I1279 at the bundle crossing region DII/S6 in the $Na_v1.4$ channel pore (Figure 7E,F). While considering the binding affinity between CBD and the $Na_v1.4$ channel, we proposed that these five binding sites probably acted as a slow-inactivation gate in the $Na_v1.4$ channel.

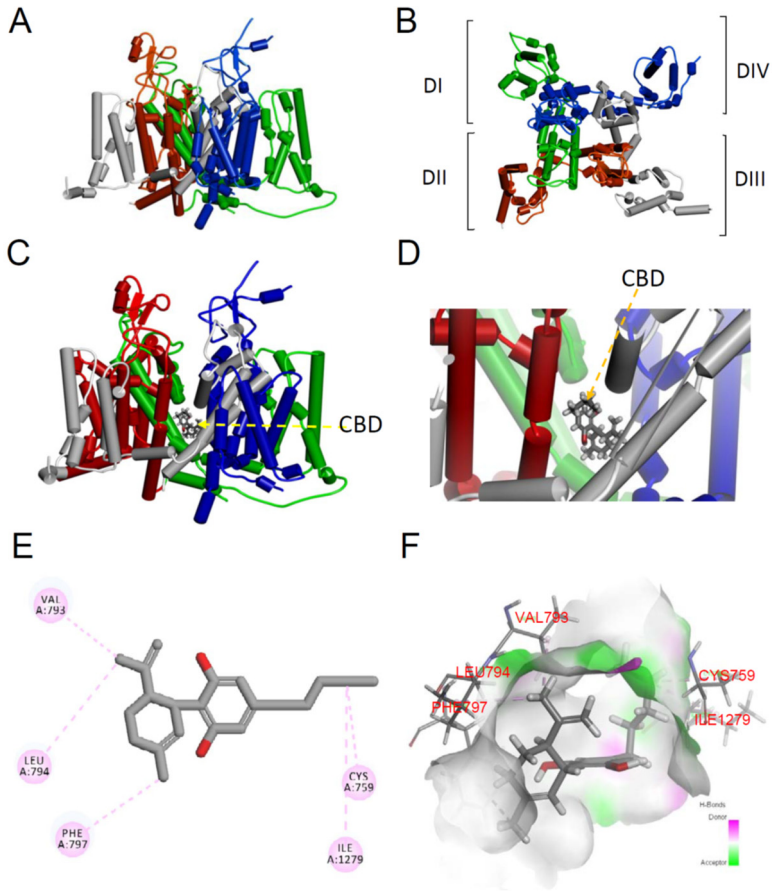

Figure 7. Homology modeling and docking interaction of the $Na_v1.4$ channel with cannabidiol. (**A**) The homology model was built based on the X-ray crystal structures of human $Na_v1.4$ channels (PDB: 6AGF) using the software Discovery Studio 2020 [37,38]. Four subunits of the $Na_v1.4$ channels homology modeling is shown. (**B**) A regional view of the extracellular side of the pore in the $Na_v1.4$ channel homology model, showing the transmembrane α-helix of the four domains. Domains I, II, III, and IV are colored in green, red, gray, and blue, respectively. (**C**) The 3D structure of the $Na_v1.4$ channel with the CBD complex using molecular docking. CBD is shown as a CPK model. (**D**) Close-up view of the $Na_v1.4$ channel with the CBD complex using molecular docking. (**E**) A 2D diagram showing the side chain of the $Na_v1.4$ channel associated with the CBD molecule. Note that Val793, Leu794, Phe797, Cys759, and Ile1279 of the $Na_v1.4$ channels are shown as the binding sites with CBD by the π alkyl interaction. (**F**) A 3D hydrogen bond surface plot at the binding site. The green color represents the conventional hydrogen bond, and the pink color represents the alkyl interaction.

4. Discussion

4.1. The Binding Kinetic Analysis of Cannabidiol with $Na_v1.4$ Channel

In summary, the current study designed a few electrophysiological protocols to explore the binding kinetics of CBD to the $Na_v1.4$ channel. First, we excluded the binding of CBD on the open state of the gate, considering that the inhibition of the activation current increased more significantly in cells with a higher resting membrane potential (−80 mV) compared to those with a low one (−120 mV). The K_{app} at −120 mV was 1341.7 μM, which is rather different from 4.1 μM at −70 mV. These findings suggest that CBD may bind to the inactivated state of the channel. As we know, two inactivated states of the voltage-gated sodium channel, fast and slow-inactivation, can be assessed according to the time lapse after depolarization. By the short period of depolarization (100 ms), the inhibition of sodium current with different concentrations of CBD did not show any significant difference (Figure 2B). Likewise, there were no disparate findings between those with or without CBD treatment (Figure 2C). These findings concordantly suggest that the fast-inactivating gate of the channel might not be the main binding site. Using the prolonged period of depolarization (18 s), we evaluate whether CBD can bind to the slow-inactivated $Na_v1.4$ channel (Figure 3). The inhibitory effect of CBD showed a marked left shift of the curve when the fraction of available channels was depicted against the different membrane potentials (Figure 3B). The higher the concentration of CBD, the more pronounced the shift. Furthermore, in addition to the left shift, the curve resumed to its original state when CBD was washed out (Figure 3C). In different concentrations, the curve with $\exp(\Delta V/k)$ against the concentration of CBD fit in a straight line using a one-to-one binding model. To further validate that CBD can bind to the slow-inactivation state of the sodium channel, the current representing the available channels recovered from slow-inactivation (the time scale for depolarization is in seconds; Figure 6A) was evaluated with different concentrations of CBD. Similar to the previous findings, the current decreased along with the increased concentration (Figure 6A). Furthermore, the significant inhibition can be observed as the time for depolarization protracted longer than 1 s, when, mainly, the $Na_v1.4$ channel was in the slow-inactivated state. Altogether, our findings reveal that CBD may bind to the $Na_v1.4$ channel in its slow-inactivated gating state. The molecular modeling suggests that five CBD binding sites on the gating hinge of the bundling crossing region in the $Na_v1.4$ channel pore were located in domain I/S6 (residues Val793, Leu794, Phe797, and Cys759) and one site of the bundling crossing region was in domain II/S6 (residue Ile1279) (Figure 7).

CBD has an inhibitory effect on the $Na_v1.4$ channel of skeletal muscles [13,39]. The IC_{50} is approximately 1.9–3.8 μM, which is in the therapeutic range [13]. A recent study indicates that CBD is a compound partitioning in lipid membranes, which indirectly alters membrane fluidity and affects voltage-gated sodium channel gating conformation [13]. Moreover, CBD was found to play a role as an open channel pore blocker in voltage-gated sodium channels and has indirect effects that are involved in modulating cell membrane elasticity [11,13]. Nevertheless, these studies did not describe how CBD inhibits the sodium current of the $Na_v1.4$ channel in different binding affinities and kinetics at the inactivated gate states. Herein, we provide evidence that CBD could bind to the slow-inactivated $Na_v1.4$ channels and the binding is selective to the slow-inactivated state with the significantly faster binding kinetics and a much higher affinity (Figures 3–6). These properties raise the intriguing possibility that CBD may have a therapeutic application for sodium channelopathies in muscles.

4.2. Clinical Implications

Our study showed that CBD binds more selectively to the slow-inactivated state with a fast-binding kinetics (>64,000 M^{-1} s^{-1}) and a high affinity (K_d of slow-inactivation is approximately 31.5 μM) (Figure 6). A previous study showed that CBD blocks the sodium current of the $Na_v1.2$ channel depending on the temperature. The lower the temperature, the stronger the potency of the inhibition [11]. In the brain slice study, a voltage-gated sodium

channel inhibitor, eslicarbazepine (ESL), enhanced the slow-inactivation of voltage-gated sodium channels [45], considering the relatively slow development ESL effect. Notably, the binding kinetics of CBD to the slow-inactivated state $Na_v1.4$ channel was slower than those for the classic Na^+ channel-inhibiting anticonvulsants diphenylhydantoin (DPH), carbamazepine (CBZ), and lamotrigine (LTG), which selectively bind to the fast-inactivated state with fast-binding kinetics [42,43,46]. DPH, CBZ, and LTG bind to a common blocking site with the two characteristic aromatic rings separated by approximately 4–5 Å [46]. Oxcarbazepine and ESL are members of the dibenzoazepine family containing the diphenyl motif [47,48]. In contrast, CBD is structurally distinct from the diphenyl compounds and contains a cyclohexene and resorcin group with a major side chain [49]. CBD contains adjacent cyclohexene and resorcinol motifs [49]. The rigid 3D structure of CBD is proposed to be more stereoselective. Molecular docking modeling revealed that CBD acts as a physical pore blocker in voltage-gated $Na_v1.4$ channels (Figure 7). The modeling predicted that five binding sites of CBD may act as part of the slow-inactivation gate (located in the residues of DI/S6 and DII/S6) (Figure 7). The fast-binding kinetics of CBD to the slow-inactivated $Na_v1.4$ channel is different from that of the DPH since it has a much slower binding kinetics. Moreover, the K_d for the binding is approximately 31.5 μM, which is higher than the therapeutic concentrations (approximately 20 μM in the central nerve system) of CBD [50,51]. The findings suggest that CBD harbors a more favorable property in clinical settings compared to DPH, CBZ, and LTG [42,43,46]. If the voltage-gated $Na_v1.4$ channel in the skeletal muscle had differential affinities to CBD, DPH, and CBZ, as that found in the neurons, the strong and steady-state inhibition of the $Na_v1.4$ channel by CBD may suggest a superiority of CBD to DPH and CBZ for the treatment of myotonia. Because the abnormal depolarization of the affected skeletal muscle cells is possibly longer than a few seconds and the repetitive discharges may protract longer than 100 ms, CBD, which favors binding of slow-inactivated sodium channels, may represent a better choice than DPH, CBZ, and LTG in muscle channelopathies caused by a dysfunctional $Na_v1.4$ channel.

According to our findings, we demonstrated that the binding affinity between CBD and the fast-inactivated $Na_v1.4$ channel is extremely low, since the K_d (K_{off}/K_{on}) of fast inactivation is greater than 117.42 μM (Figure 5). CBD binds more selectively to the slow-inactivated $Na_v1.4$ channel with a faster binding rate (>64,000 M^{-1} s^{-1}) and a lower K_d, of approximately 31.5 μM, which is above the highest therapeutic concentration range. The K_d of the binding between the slow-inactivation sodium channel and DPH is approximately 14 μM, which is below the therapeutic concentrations [52]. Therefore, CBD may be superior to DPH, while the myotonia discharges are characterized by more positive membrane voltages during the burst intervals, driving more $Na_v1.4$ channels into the slow-inactivated state. In addition, physiological burst discharges are presumably less affected by CBD than by DPH. Although CBD and the other classical voltage-gated sodium channel blockers similarly target $Na_v1.2$ channels [13], they are pharmacologically distinct anti-myotonia medications. Given the different burst intervals in the same patient, combining CBD with other voltage-gated sodium channel blockers (such as DPH, CBZ, and LTG) to treat myotonia in $Na_v1.4$ muscle channelopathies may increase its effectiveness

4.3. Same Molecular Structure but Different Biological Functions in Cannabidiol and Tetrahydrocannabinol

In addition to CBD, tetrahydrocannabinol (THC) can also be extracted from hemp or cannabis. Both compounds interact with the endocannabinoid system; however, they have very different effects. The molecular structures for CBD and THC are the same, with 21 carbon atoms, 30 hydrogen atoms, and 2 oxygen atoms [12]. A slight difference in how the atoms are arranged accounts for the differing effects on the body. Both CBD and THC interact with cannabinoid receptors. The interaction affects the release of neurotransmitters in the brain which are responsible for relaying messages between cells and have roles in pain, immune function, stress, and sleep. Despite their similar chemical structures, CBD and THC do not have the same psychoactive effects [12,53]. CBD does not produce the high emotions associated with THC [12,53]. Nevertheless, CBD was effective in ameliorating

anxiety, depression, and seizures. THC binds with the cannabinoid 1 (CB1) receptors in the brain. It produces a high or sense of euphoria. CBD can also bind to CB1 receptors but is very weak in binding. It needs THC for the binding and [13], in turn, CBD can help reduce some of the unwanted psychoactive effects of THC, such as euphoria or sedation. Given that CBD has a lower affinity for the endocannabinoid receptors than THC [13,54], several studies suggested that the anticonvulsant effects of THC and CBD in maximal electroshock and pilocarpine models occur with different mechanisms [13,50]. The THC activity is mostly through the CB1 receptor; however, the anticonvulsant effects of CBD are not [13]. These findings have inspired the growth of CB1- and CB2-independent focused research in epilepsy model.

5. Conclusions

CBD is able to relieve myotonia caused by sodium channelopathy, which results from high from high frequency repetitive discharge of the muscle membrane. Findings from the current study elucidate the binding kinetics of CBD onto the voltage-gated $Na_v1.4$ channel of the muscle. CBD selectively binds to the $Na_v1.4$ channel in its slow-inactivated state. The highly selective and efficient binding of CBD onto the slow-inactivated $Na_v1.4$ channel provides novel therapeutic avenues to treat myotonia caused by sodium channelopathy.

Supplementary Materials: The following are available online at https://www.mdpi.com/article/10.3390/biomedicines9091141/s1. Figure S1: The area under the recovery time course curves obtained from depolarization at −10 and −80 mV.

Author Contributions: C.-W.H. designed and performed the experiments. C.-W.H. and M.-J.L. were involved in the analysis and interpretation of the data, and participated in writing the manuscript. P.-C.L. and J.-L.C. performed the modeling using CDOCKER program in the DS 2020 software. All authors have read and agreed to the published version of the manuscript.

Funding: This work was supported by the grants MOST 109-2314-B-002-121-MY3 to M.-J.L., MOST 107-2320-B-037-004 to C.-W.H., MOST 108-2320-B-037-032 to C.-W.H., MOST 109-2320-B-037-009 to C.-W.H. and MOST 110-2320-B-037-004 to C.-W.H. from the Ministry of Science and Technology, Taiwan. Other supports from Kaohsiung Medical University (KMU-Q108004 and KMU-Q107007 to C.-W.H.) and (KMUH106-M608 to P.-C.L.) are also acknowledged. We are also thankful for the support from the National Taiwan University Hospital (NTUH.109-004528).

Acknowledgments: We thank the third common laboratory at NTUH for providing the facilities and techniques. We also thank Kuan-Wen Chen and Tzu-Mao Hung in Molecular Science and Digital Innovation Center, Genetics Generation Advancement Corporation (GGA Corp.), for performing the molecular docking study.

Conflicts of Interest: The authors declare no conflict of interest.

References

1. Catterall, W.A. Voltage-gated sodium channels at 60: Structure, function and pathophysiology. *J. Physiol.* **2012**, *590*, 2577–2589. [CrossRef]
2. Ghovanloo, M.R.; Aimar, K.; Ghadiry-Tavi, R.; Yu, A.; Ruben, P.C. Physiology and Pathophysiology of Sodium Channel Inactivation. *Curr. Top. Membr.* **2016**, *78*, 479–509. [CrossRef]
3. Ghovanloo, M.R.; Atallah, J.; Escudero, C.A.; Ruben, P.C. Biophysical Characterization of a Novel SCN5A Mutation Associated with an Atypical Phenotype of Atrial and Ventricular Arrhythmias and Sudden Death. *Front. Physiol.* **2020**, *11*, 610436. [CrossRef] [PubMed]
4. Ghovanloo, M.R.; Ruben, P.C. Say Cheese: Structure of the Cardiac Electrical Engine Is Captured. *Trends Biochem. Sci.* **2020**, *45*, 369–371. [CrossRef] [PubMed]
5. Fouda, M.A.; Ghovanloo, M.R.; Ruben, P.C. Cannabidiol protects against high glucose-induced oxidative stress and cytotoxicity in cardiac voltage-gated sodium channels. *Br. J. Pharmacol.* **2020**, *177*, 2932–2946. [CrossRef] [PubMed]
6. Kol, S.; Turrell, B.R.; de Keyzer, J.; van der Laan, M.; Nouwen, N.; Driessen, A.J. YidC-mediated membrane insertion of assembly mutants of subunit c of the F1F0 ATPase. *J. Biol. Chem.* **2006**, *281*, 29762–29768. [CrossRef] [PubMed]
7. David, M.; Martinez-Marmol, R.; Gonzalez, T.; Felipe, A.; Valenzuela, C. Differential regulation of Na(v)beta subunits during myogenesis. *Biochem. Biophys. Res. Commun.* **2008**, *368*, 761–766. [CrossRef] [PubMed]

8. Lee, S.; Goodchild, S.J.; Ahern, C.A. Local anesthetic inhibition of a bacterial sodium channel. *J. Gen. Physiol.* **2012**, *139*, 507–516. [CrossRef]
9. Gamal El-Din, T.M.; Lenaeus, M.J.; Zheng, N.; Catterall, W.A. Fenestrations control resting-state block of a voltage-gated sodium channel. *Proc. Natl. Acad. Sci. USA* **2018**, *115*, 13111–13116. [CrossRef]
10. Pan, X.; Li, Z.; Zhou, Q.; Shen, H.; Wu, K.; Huang, X.; Chen, J.; Zhang, J.; Zhu, X.; Lei, J.; et al. Structure of the human voltage-gated sodium channel Nav1.4 in complex with beta1. *Science* **2018**, *362*, eaau2486. [CrossRef]
11. Ghovanloo, M.R.; Choudhury, K.; Bandaru, T.S.; Fouda, M.A.; Rayani, K.; Rusinova, R.; Phaterpekar, T.; Nelkenbrecher, K.; Watkins, A.R.; Poburko, D.; et al. Cannabidiol inhibits the skeletal muscle Nav1.4 by blocking its pore and by altering membrane elasticity. *J. Gen. Physiol.* **2021**, *153*, e202012701. [CrossRef] [PubMed]
12. Ghovanloo, M.R.; Abdelsayed, M.; Peters, C.H.; Ruben, P.C. A Mixed Periodic Paralysis & Myotonia Mutant, P1158S, Imparts pH-Sensitivity in Skeletal Muscle Voltage-gated Sodium Channels. *Sci. Rep.* **2018**, *8*, 6304. [CrossRef] [PubMed]
13. Ghovanloo, M.R.; Shuart, N.G.; Mezeyova, J.; Dean, R.A.; Ruben, P.C.; Goodchild, S.J. Inhibitory effects of cannabidiol on voltage-dependent sodium currents. *J. Biol. Chem.* **2018**, *293*, 16546–16558. [CrossRef]
14. Lossin, C.; George, A.L., Jr. Myotonia congenita. *Adv. Genet.* **2008**, *63*, 25–55. [CrossRef]
15. Huang, S.; Zhang, W.; Chang, X.; Guo, J. Overlap of periodic paralysis and paramyotonia congenita caused by SCN4A gene mutations two family reports and literature review. *Channels* **2019**, *13*, 110–119. [CrossRef] [PubMed]
16. Holzherr, B.; Lehmann-Horn, F.; Kuzmenkina, E.; Fan, C.; Jurkat-Rott, K. A gating model for wildtype and R1448H Nav1.4 channels in paramyotonia. *Acta Myol.* **2014**, *33*, 22–33. [PubMed]
17. Hsu, W.C.; Huang, Y.C.; Wang, C.W.; Hsueh, C.H.; Lai, L.P.; Yeh, J.H. Paralysis periodica paramyotonica caused by SCN4A Arg1448Cys mutation. *J. Formos. Med. Assoc.* **2006**, *105*, 503–507. [CrossRef]
18. Ke, Q.; Ye, J.; Tang, S.; Wang, J.; Luo, B.; Ji, F.; Zhang, X.; Yu, Y.; Cheng, X.; Li, Y. N1366S mutation of human skeletal muscle sodium channel causes paramyotonia congenita. *J. Physiol.* **2017**, *595*, 6837–6850. [CrossRef] [PubMed]
19. Mazon, M.J.; Barros, F.; De la Pena, P.; Quesada, J.F.; Escudero, A.; Cobo, A.M.; Pascual-Pascual, S.I.; Gutierrez-Rivas, E.; Guillen, E.; Arpa, J.; et al. Screening for mutations in Spanish families with myotonia. Functional analysis of novel mutations in CLCN1 gene. *Neuromuscul. Disord.* **2012**, *22*, 231–243. [CrossRef] [PubMed]
20. Lehmann-Horn, F.; Jurkat-Rott, K.; Rudel, R.; Ulm Muscle, C. Diagnostics and therapy of muscle channelopathies—Guidelines of the Ulm Muscle Centre. *Acta Myol.* **2008**, *27*, 98–113. [PubMed]
21. Cannon, S.C. Pathomechanisms in channelopathies of skeletal muscle and brain. *Annu. Rev. Neurosci.* **2006**, *29*, 387–415. [CrossRef] [PubMed]
22. Loussouarn, G.; Sternberg, D.; Nicole, S.; Marionneau, C.; Le Bouffant, F.; Toumaniantz, G.; Barc, J.; Malak, O.A.; Fressart, V.; Pereon, Y.; et al. Physiological and Pathophysiological Insights of Nav1.4 and Nav1.5 Comparison. *Front. Pharmacol.* **2015**, *6*, 314. [CrossRef] [PubMed]
23. Beard, J.M.; Shockett, P.E.; O'Reilly, J.P. Substituted cysteine scanning in D1-S6 of the sodium channel hNav1.4 alters kinetics and structural interactions of slow inactivation. *Biochim. Biophys. Acta Biomembr.* **2020**, *1862*, 183129. [CrossRef] [PubMed]
24. Vite, C.H. Myotonia and disorders of altered muscle cell membrane excitability. *Vet. Clin. N. Am. Small Anim. Pract.* **2002**, *32*, 169–187. [CrossRef]
25. Pagliarani, S.; Lucchiari, S.; Scarlato, M.; Redaelli, E.; Modoni, A.; Magri, F.; Fossati, B.; Previtali, S.C.; Sansone, V.A.; Lecchi, M.; et al. Sodium Channel Myotonia Due to Novel Mutations in Domain I of Nav1.4. *Front. Neurol.* **2020**, *11*, 255. [CrossRef]
26. Devinsky, O.; Marsh, E.; Friedman, D.; Thiele, E.; Laux, L.; Sullivan, J.; Miller, I.; Flamini, R.; Wilfong, A.; Filloux, F.; et al. Cannabidiol in patients with treatment-resistant epilepsy: An open-label interventional trial. *Lancet. Neurol.* **2016**, *15*, 270–278. [CrossRef]
27. Patel, R.R.; Barbosa, C.; Brustovetsky, T.; Brustovetsky, N.; Cummins, T.R. Aberrant epilepsy-associated mutant Nav1.6 sodium channel activity can be targeted with cannabidiol. *Brain* **2016**, *139*, 2164–2181. [CrossRef]
28. Petrovici, A.R.; Simionescu, N.; Sandu, A.I.; Paraschiv, V.; Silion, M.; Pinteala, M. New Insights on Hemp Oil Enriched in Cannabidiol: Decarboxylation, Antioxidant Properties and In Vitro Anticancer Effect. *Antioxidants* **2021**, *10*, 738. [CrossRef]
29. Campos, A.C.; Moreira, F.A.; Gomes, F.V.; Del Bel, E.A.; Guimaraes, F.S. Multiple mechanisms involved in the large-spectrum therapeutic potential of cannabidiol in psychiatric disorders. *Philos. Trans. R. Soc. Lond. B Biol. Sci.* **2012**, *367*, 3364–3378. [CrossRef]
30. Black, N.; Stockings, E.; Campbell, G.; Tran, L.T.; Zagic, D.; Hall, W.D.; Farrell, M.; Degenhardt, L. Cannabinoids for the treatment of mental disorders and symptoms of mental disorders: A systematic review and meta-analysis. *Lancet Psychiatry* **2019**, *6*, 995–1010. [CrossRef]
31. VanDolah, H.J.; Bauer, B.A.; Mauck, K.F. Clinicians' Guide to Cannabidiol and Hemp Oils. *Mayo Clin. Proc.* **2019**, *94*, 1840–1851. [CrossRef] [PubMed]
32. Itin, C.; Barasch, D.; Domb, A.J.; Hoffman, A. Prolonged oral transmucosal delivery of highly lipophilic drug cannabidiol. *Int. J. Pharm.* **2020**, *581*, 119276. [CrossRef] [PubMed]
33. Itin, C.; Domb, A.J.; Hoffman, A. A meta-opinion: Cannabinoids delivered to oral mucosa by a spray for systemic absorption are rather ingested into gastro-intestinal tract: The influences of fed/fasting states. *Expert Opin. Drug Deliv.* **2019**, *16*, 1031–1035. [CrossRef]

34. Devinsky, O.; Cross, J.H.; Wright, S. Trial of Cannabidiol for Drug-Resistant Seizures in the Dravet Syndrome. *N. Engl. J. Med.* **2017**, *377*, 699–700. [CrossRef] [PubMed]
35. Devinsky, O.; Cross, J.H.; Laux, L.; Marsh, E.; Miller, I.; Nabbout, R.; Scheffer, I.E.; Thiele, E.A.; Wright, S.; Cannabidiol in Dravet Syndrome Study Group. Trial of Cannabidiol for Drug-Resistant Seizures in the Dravet Syndrome. *N. Engl. J. Med.* **2017**, *376*, 2011–2020. [CrossRef]
36. Devinsky, O.; Patel, A.D.; Cross, J.H.; Villanueva, V.; Wirrell, E.C.; Privitera, M.; Greenwood, S.M.; Roberts, C.; Checketts, D.; VanLandingham, K.E.; et al. Effect of Cannabidiol on Drop Seizures in the Lennox-Gastaut Syndrome. *N. Engl. J. Med.* **2018**, *378*, 1888–1897. [CrossRef] [PubMed]
37. Huang, C.W.; Lai, H.J.; Lin, P.C.; Lee, M.J. Changes of Resurgent Na(+) Currents in the Nav1.4 Channel Resulting from an SCN4A Mutation Contributing to Sodium Channel Myotonia. *Int. J. Mol. Sci.* **2020**, *21*, 2593. [CrossRef]
38. Huang, C.W.; Lai, H.J.; Lin, P.C.; Lee, M.J. Changes in Resurgent Sodium Current Contribute to the Hyperexcitability of Muscles in Patients with Paramyotonia Congenita. *Biomedicines* **2021**, *9*, 51. [CrossRef]
39. Sait, L.G.; Sula, A.; Ghovanloo, M.R.; Hollingworth, D.; Ruben, P.C.; Wallace, B.A. Cannabidiol interactions with voltage-gated sodium channels. *eLife* **2020**, *9*, 9. [CrossRef]
40. Kuo, C.C.; Bean, B.P. Na+ channels must deactivate to recover from inactivation. *Neuron* **1994**, *12*, 819–829. [CrossRef]
41. Peng, Y.S.; Wu, H.T.; Lai, Y.C.; Chen, J.L.; Yang, Y.C.; Kuo, C.C. Inhibition of neuronal Na(+) currents by lacosamide: Differential binding affinity and kinetics to different inactivated states. *Neuropharmacology* **2020**, *179*, 108266. [CrossRef] [PubMed]
42. Kuo, C.C.; Chen, R.S.; Lu, L.; Chen, R.C. Carbamazepine inhibition of neuronal Na+ currents: Quantitative distinction from phenytoin and possible therapeutic implications. *Mol. Pharmacol.* **1997**, *51*, 1077–1083. [CrossRef] [PubMed]
43. Kuo, C.C.; Lu, L. Characterization of lamotrigine inhibition of Na+ channels in rat hippocampal neurones. *Br. J. Pharmacol.* **1997**, *121*, 1231–1238. [CrossRef] [PubMed]
44. Kuo, C.C. A common anticonvulsant binding site for phenytoin, carbamazepine, and lamotrigine in neuronal Na+ channels. *Mol. Pharmacol.* **1998**, *54*, 712–721. [PubMed]
45. Hebeisen, S.; Pires, N.; Loureiro, A.I.; Bonifacio, M.J.; Palma, N.; Whyment, A.; Spanswick, D.; Soares-da-Silva, P. Eslicarbazepine and the enhancement of slow inactivation of voltage-gated sodium channels: A comparison with carbamazepine, oxcarbazepine and lacosamide. *Neuropharmacology* **2015**, *89*, 122–135. [CrossRef]
46. Kuo, C.C.; Bean, B.P. Slow binding of phenytoin to inactivated sodium channels in rat hippocampal neurons. *Mol. Pharmacol.* **1994**, *46*, 716–725.
47. Kuo, C.C.; Huang, R.C.; Lou, B.S. Inhibition of Na(+) current by diphenhydramine and other diphenyl compounds: Molecular determinants of selective binding to the inactivated channels. *Mol. Pharmacol.* **2000**, *57*, 135–143.
48. Keating, G.M. Eslicarbazepine acetate: A review of its use as adjunctive therapy in refractory partial-onset seizures. *CNS Drugs* **2014**, *28*, 583–600. [CrossRef]
49. Zaccara, G.; Perucca, P.; Loiacono, G.; Giovannelli, F.; Verrotti, A. The adverse event profile of lacosamide: A systematic review and meta-analysis of randomized controlled trials. *Epilepsia* **2013**, *54*, 66–74. [CrossRef]
50. Burstein, S. Cannabidiol (CBD) and its analogs: A review of their effects on inflammation. *Bioorg. Med. Chem.* **2015**, *23*, 1377–1385. [CrossRef]
51. Devinsky, O.; Cilio, M.R.; Cross, H.; Fernandez-Ruiz, J.; French, J.; Hill, C.; Katz, R.; Di Marzo, V.; Jutras-Aswad, D.; Notcutt, W.G.; et al. Cannabidiol: Pharmacology and potential therapeutic role in epilepsy and other neuropsychiatric disorders. *Epilepsia* **2014**, *55*, 791–802. [CrossRef] [PubMed]
52. Deiana, S.; Watanabe, A.; Yamasaki, Y.; Amada, N.; Arthur, M.; Fleming, S.; Woodcock, H.; Dorward, P.; Pigliacampo, B.; Close, S.; et al. Plasma and brain pharmacokinetic profile of cannabidiol (CBD), cannabidivarine (CBDV), Delta(9)-tetrahydrocannabivarin (THCV) and cannabigerol (CBG) in rats and mice following oral and intraperitoneal administration and CBD action on obsessive-compulsive behaviour. *Psychopharmacology* **2012**, *219*, 859–873. [CrossRef] [PubMed]
53. Pertwee, R.G. The diverse CB1 and CB2 receptor pharmacology of three plant cannabinoids: Delta9-tetrahydrocannabinol, cannabidiol and delta9-tetrahydrocannabivarin. *Br. J. Pharmacol.* **2008**, *153*, 199–215. [CrossRef] [PubMed]
54. Straiker, A.; Dvorakova, M.; Zimmowitch, A.; Mackie, K. Cannabidiol Inhibits Endocannabinoid Signaling in Autaptic Hippocampal Neurons. *Mol. Pharmacol.* **2018**, *94*, 743–748. [CrossRef] [PubMed]